ELSEVIER

Ceramics International 27 (2001) 621–628

CERAMICS INTERNATIONAL

www.elsevier.com/locate/ceramint

Effect of Y_2O_3 and Yb_2O_3 on the microstructure and mechanical properties of silicon nitride

Horng-Hwa Lu, Jow-Lay Huang *

Department of Materials Science and Engineering, National Cheng-Kung University, Tainan 701, Taiwan, ROC

Received 28 August 2000; received in revised form 14 September 2000; accepted 18 November 2000

Abstract

The effect of Y_2O_3 and Yb_2O_3 on the microstructure and mechanical properties of silicon nitride was investigated. The effect of heat-treatment on the crystallization of grain boundary phases and on the high-temperature strength was also studied. Sinterability and α to β phase transformation of silicon nitride with Y_2O_3 were more pronounced than that with Yb_2O_3, for the same additive content. A wider grain size distribution and a larger average grain size were observed in the specimens with Y_2O_3. The specimens with Yb_2O_3 showed higher flexure strength, hardness and fracture toughness owing to a more frequent pullout of grains. Strength retention of silicon nitride at elevated temperatures was attributed to the crystallization and refractoriness of the grain boundary phases.

Keywords: B. Microstructure; C. Mechanical properties; D. Silicon nitride; Sintering additives

1. Introduction

Silicon nitride is one of the most promising structural materials for high-temperature applications because of its excellent strength and toughness at elevated temperatures, good thermal shock resistance and chemical stability, and low coefficient of thermal expansion [1–3]. However, its densification is relatively difficult by the sintering process because of the 70% covalent and 30% ionic in Si–N bonds [4]. The use of rare-earth oxide additives to provide a liquid medium for sintering is therefore required for obtaining high-density Si_3N_4 [5,6].

Some metal oxides such as MgO, Al_2O_3, Y_2O_3, Re_2O_3 have been used as sintering additives for the densification of Si_3N_4 [7–10]. The liquid formed via the chemical reactions between the additives and SiO_2 on the Si_3N_4 could enhance the diffusivity of atoms during sintering. Most of the liquid phase formed amorphous films at the grain boundaries, grain junctions or pockets upon cooling. The compositions of the secondary boundary phases have a substantial influence on the flow behavior, microstructural characteristics and high temperature properties of Si_3N_4 [11,12].

To improve the high temperature properties of Si_3N_4, the residual glass phase can be minimized or crystallized by selecting appropriate types of sintering aids or via after-heat treatments [13,14]. For example, it has been previously reported that Si_3N_4 sintered with Dy_2O_3 exhibited good creep resistance, while that with Yb_2O_3 had high strength at elevated temperatures [14,15]. It has also been reported that through the crystallization of grain boundary phases and formation of highly viscous amorphous films, the high temperature strength of Si_3N_4 could preserve up to 90% of its room-temperature strength [15].

Y_2O_3 has been a promising sintering additive for both pressureless and gas-pressure sintered Si_3N_4 [7,8,13–16]. Although the microstructure and mechanical properties of sintered Si_3N_4 containing Y_2O_3,, Re_2O_3, Al_2O_3 have been previously reported [3,6,7–10], the effects of Yb_2O_3–Al_2O_3 on the developed microstructure and elevated-temperature properties still need further research for good understanding.

One major purpose of this study was to investigate and compare the effects of Y_2O_3 and Yb_2O_3 on the developed microstructure and mechanical properties of Si_3N_4. In addition, the effects of post-heat treatment on the developed phase, high-temperature flexural strength and the aspect of fractured surfaces were also studied.

Corresponding author. Fax: +886-6-2763586.
E-mail address: jlh888@mail.ncku.edu.tw (J-L. Huang).

0272-8842/01/$20.00
PII: S0272-8842(01)00008-6

2. Experimental procedure

2.1. Sample preparation

Si_3N_4 powders (UBE Corp., SN-E10, 0.2 μm) were mixed with Y_2O_3 (5603, Molycorp, 1.8 μm) or Yb_2O_3 (Cerac, Y-1015) in a polyethylene bottle with high purity Si_3N_4 balls and ethanol for 24 h. The sample designations and corresponding compositions are expressed in Table 1. The slurry was dried in a rotary evaporator and ground with an alumina mortar and pestle followed by screening through a −200 mesh screen. Powders were then die-pressed uniaxially at 10 MPa to form a 5×5×50 mm green compact and cold-pressed isostatically at 100 MPa for 1.5 min. Samples were subsequently embedded in powder bed in a graphite crucible and sintered in a graphite furnace at 1800°C for 1 h under 1 MPa N_2. The covering powders consisted of 50% BN and 50% Si_3N_4 (including sintering additives) by mass.

In order to compare the effects of sintering additives on the density and phase transformation of Si_3N_4 at various sintering temperatures, samples were held for 5 min at different temperatures in the range between 1400 and 1800°C and then cooled down before conducting phase analysis and density measurement. In order to investigate the effects of post-sintering on the microstructure and mechanical behaviors of silicon nitride, some as-sintered samples were further heat treated at 1450°C for 24 h in 0.1 MPa N_2.

2.2. Microstructural analysis

Sintered specimens were polished to 1 μm, chemically etched in NaOH, melted at 350°C for 1.5 min and coated with Au before SEM examination (Hitachi S-2500). In order to characterize quantitatively the grain morphology of sintered Si_3N_4, the grain length and area of over 2000 grains were measured by the image analyzer associated with Optimas software (Bioscan Inc., Edmons, Washington, USA) and calculated following the statistical derivation by Woetting et al. [17] The grain diameter and apparent aspect ratio of each grain were determined from the area/length and length/diameter, respectively. The 'true' aspect ratio was obtained from the frequency distribution of the aspect ratio, which was visible in a microsection, subsequently selecting the value as a_{95}. In other words, 5% of all visible grains exhibited a higher aspect ratio while 95% demonstrated a lower aspect ratio than the 'true' aspect ratio.

Table 1
Designations and corresponding compositions of samples examined

Designations	Compositions
SY	Si_3N_4 + 6 wt.% Y_2O_3 + 2 wt.% Al_2O_3
SYb	Si_3N_4 + 6 wt.% Yb_2O_3 + 2 wt.% Al_2O_3

TEM specimens were ultrasonically machined from sintered bars, dimpled to 25 μm and ion milled by argon ions before scrutiny. An energy dispersive spectrometer (EDS) associated with transmission electron microscope (TEM, Jeol 3010) was used for elemental analysis.

2.3. Characterization and mechanical properties

Phases were identified by X-ray diffractometer (XRD, Rigaku D/Max-IIB). Samples were scanned from 10 to 80° with a scanning rate of 4°/min, and from 30 to 40° with a particularly slow scanning rate of 0.5°/min. The phase ratio of $\alpha/(\alpha+\beta)$ was determined from the X-ray peaks by a technique derived by Gazzara and Messier [18].

The bulk density of sintered specimens was measured by the Archimede's method. The relative density was calculated on the basis of the theoretical density derived from each individual constituent and its content.

Test samples were machined into bars of dimensions 3×4×45 mm (ASTM E855-81) and then polished to 1 μm before a four-point bending test was conducted at a loading rate of 0.5 mm/min on a universal testing machine (Instron 8511). Sample edges were chamfered to minimize possible interference coming from stress concentration. The outer and inner spans were 40 and 20 mm, respectively.

High temperature strength was determined in a $MoSi_2$ furnace assembled to a universal-testing machine. Samples were held at temperatures for 5 min at a heating rate of 10°C/min on SiC test fixture. Each strength value was calculated from the average of more than six samples.

Fracture toughness was determined by the single-edge-precracked beam (SEPB) method[19] on a universal-testing machine. The test procedure and sample preparation was similar to that of a four-point bend test. An initial precrack of 1 mm in depth was cut using a diamond blade (0.15 mm in thickness). Each data point represents an average of six tests.

3. Results and discussion

3.1. Sinterability and phase transformation

Fig. 1 presents the relative density of SY and SYb samples sintered at temperatures in the range of 1400–1800°C. The density of SY samples was consistently higher than that of SYb at temperatures below 1600°C. However, there was no evident difference in density at temperatures above 1700°C. Further experiments showed that both specimens reached a relative density of more than 99% after sintering at 1800°C. The liquid formation temperature and the flowability of grain boundary phase in each sample may have a role in densification [3].

The results of X-ray analysis for SY and SYb samples as a function of sintering temperature are shown in

Fig. 2. Results indicated that the β-phase content increased invariably with sintering temperature. This was especially evident at temperatures above 1550 where the solution-precipitation occurred [20,21]. Further experiments showed that all the α phase was transformed into β phase after being sintered at 1800°C for both samples.

The β-phase content of SY was consistently higher than that of SYb at all temperatures. It was previously suggested that the α to β conversion in Si_3N_4 follows the first-order kinetics, i.e. the conversion is controlled by a solution-diffusion–reprecipitation mechanism [22]. Although results in Figs. 1 and 2 indicated that both the densification behavior and α to β transformation were affected by the type of sintering aids and temperature, previous investigation suggested that the transformation of α to β and the densification process are not directly correlated [22,23].

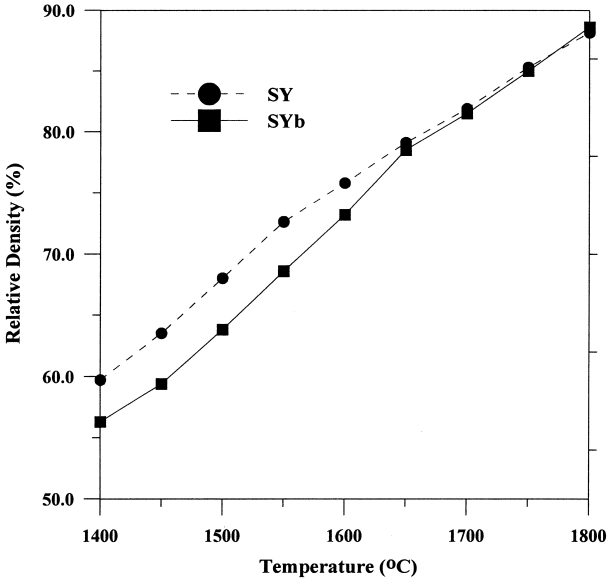

Fig. 1. Relative density of SY and SYb samples sintered at 1400 – 1800°C. All samples were sintered under 1 MPa N_2 for 5 min.

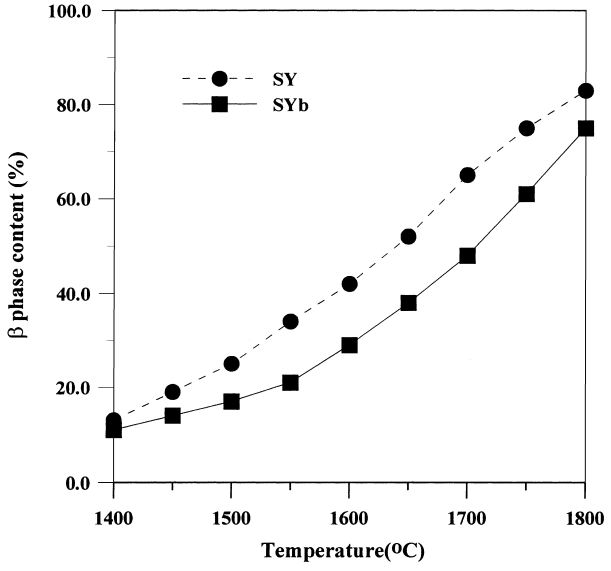

Fig. 2. β-Phase content as a function of sintering temperature in SY and SYb specimens. Samples were sintered under 1 MPa N_2 for 5 min.

It was formerly suggested that the presence of liquid phase during sintering also acts as a solvent necessary for the α to β phase transformation in silicon nitride [5,6]. The glass transformation temperature of Y_2O_3–Al_2O_3–SiO_2 was found to be lower than that of the Yb_2O_3–Al_2O_3–SiO_2 system[24] when samples with the same amount of sintering additives were compared. This indicated that the liquid phase could be generated earlier and the viscosity could be lower in Y_2O_3–Al_2O_3–SiO_2 than in the Yb_2O_3–Al_2O_3–SiO_2 system during sintering. This was probably the reason for greater α to β conversion and higher relative density observed in SY specimens as shown in Figs. 1 and 2.

3.2. Microstructural characteristics

Typical SEM micrographs of SY and SYb samples sintered at 1800 for 1 h under 10 atm N_2 are shown in Fig. 3. Elongated grains embedded in relatively small matrix grains can be observed in Fig. 3(a) and (b). Results indicated that the overall grain size of SY samples was substantially larger than that of SYb ones. The microstructural evolutions were shown to be strongly influenced by the type of sintering aids [6,9].

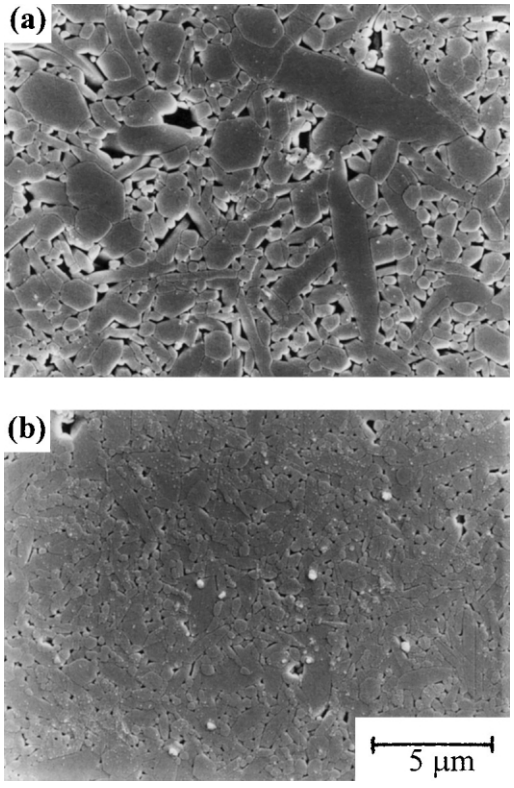

Fig. 3. Typical microstructures of (a) SY and (b) SYb samples sintered at 1800°c for 1 h under 10 atm N_2.

The grain width distribution of SY and SYb specimens were determined as shown in Fig. 4. Results revealed that wider grain width distribution and larger grains were observed in SY samples in comparison with SYb. The average grain width was further determined by taking the mean width at half of the maximum frequency. Both the average grain width and aspect ratio of SY were larger than those of SYb samples as shown in Table 2.

Parameters controlling the morphology of elongated β-phase Si_3N_4 grains were discussed previously. They include the sintering additives [6,9,25], sintering conditions [26], and the amount and size distribution of β-phase Si_3N_4 in the starting powders [21,27,28]. It is generally accepted that the β-phase Si_3N_4 particles could act as nuclei and promote grain growth during sintering process [21,28]. The relatively larger grain width and wider grain width distribution in SY specimens is possibly correlated with the amount of α to β conversion at the initial and intermediate stages of sintering (Fig. 2).

3.3. Mechanical properties

The room-temperature flexure strength and hardness of SYb specimens were higher than those of SY specimens as summarized in Table 2. This was probably due to the smaller grain size (Fig. 3) and characteristics of grain boundary phases formed in SYb samples [15,29,30].

Results in Table 2 showed that the fracture toughness of SYb (11.8 MPa $m^{1/2}$) samples was substantially greater than that of SY (6.2 MPa $m^{1/2}$) ones. The SEM micrographs revealing the fractured surfaces of as sintered SY and SYb specimens are shown in Fig. 5. To achieve toughening of Si_3N_4 by crack bridging or crack deflection mechanisms, the formation of large elongated grains is necessary [2]. However, the existence of the elongated grains does not guarantee the occurrence of these toughening mechanisms unless the cracks propagate along the grain interfaces. The observations shown in Fig. 5 indicated the occurrence of intergranular fracture in both samples, and more pullout of grains was detected in SYb samples than in SY ones.

Table 2
Characteristic of microstructure and mechanical properties of SY and SYb specimens

Properties	Specimens	
	SY	SYb
Relative density (%)	99.4	99.2
Average grain size (μm)	0.252	0.204
Aspect ratio	6.27	5.85
4-p Bending strength (MPa)	880.5±51	950±46
Fracture toughness (MPa $m^{1/2}$)	6.2±0.3	11.8±0.9
Hardness (HV)	1354±32	1526±28

For the intergranular fracture mode, debonding at the interface between the grains and grain boundary phase should occur. The interfacial debonding energy was reported to be directly influenced by the chemical bonding between the grain boundary phase and the grains, and also by the residual stress imposed on the interface due to thermal expansion mismatch [25,29,31]. Tajima [25] observed a significant decrease in the toughness of MgO/ZrO_2-doped Si_3N_4 by the addition of small amounts of Al_2O_3, despite the fact that the grain size and morphology were not evidently changed. The higher fracture toughness in SYb could be due to its lower interfacial

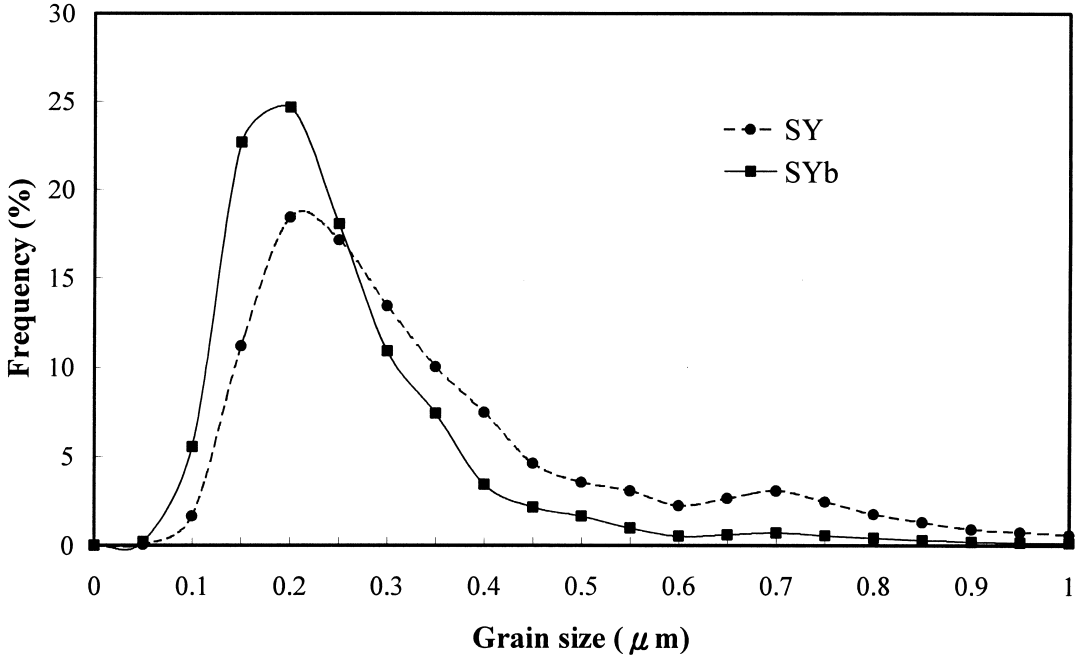

Fig. 4. Grain width distribution of SY and SYb specimens. Samples were sintered at 1800°C for 1 h in 1 MPa N_2.

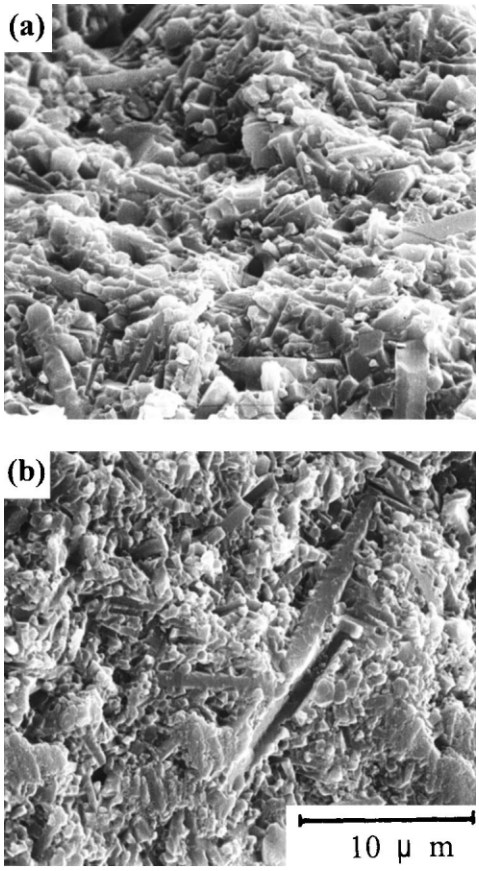

Fig. 5. Fractured surfaces of as-sintered (a) SY and (b) SYb specimens. Samples were sintered at 1800°C for 1 h in 1 MPa N_2.

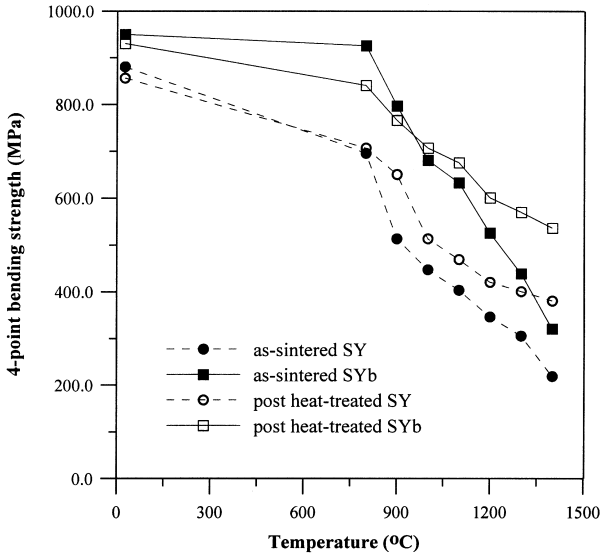

Fig. 6. Flexural strength of as-sintered and post heat-treated SY and SYb specimens as a function of test temperature. Samples were sintered at 1800°C for 1 h in 1 MPa N_2. Some were further post heat-treated at 1450°C for 24 h in 0.1 MPa N_2.

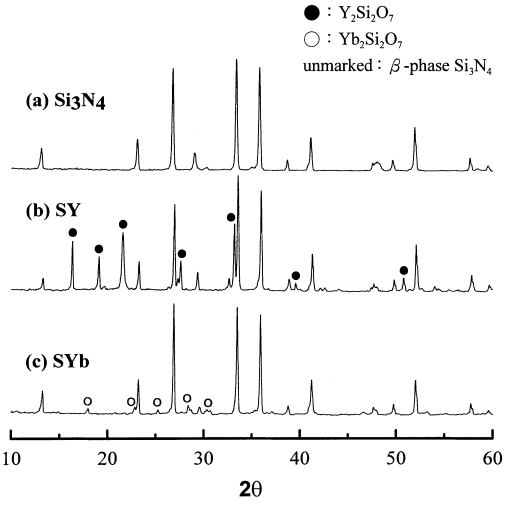

Fig. 7. Typical XRD patterns of (a) as-sintered SYb specimens, (b) post heat-treated SY specimens, and (c) post heat-treated SYb specimens.

bonding energy resulting from the different grain boundary phases. This was also probably why a larger amount of grain pullout was observed in SYb samples than in SY ones (Fig. 5).

The high temperature strength of as-sintered SY and SYb specimens is shown in Fig. 6. The strength of as-sintered SYb samples was consistently higher than that of SY although they both degraded at elevated temperatures. The high temperature bending strength of post heat-treated specimens is also shown in Fig. 6. Similar to that of as-sintered samples, the SYb specimens exhibited greater hot strength than SY ones. In addition, the high temperature strength of post-heated samples is substantially higher than that of as-sintered ones. It suggested that the degradation of strength at high temperature could be effectively reduced after heat treatment.

Phase analysis was conducted on as-sintered SYb (Fig. 7a), post heat-treated SY and SYb (Fig. 7b and c) samples. Results of XRD patterns revealed that only β-Si_3N_4 phase was detected in as-sintered samples. However, $Yb_2Si_2O_7$ and $Y_2Si_2O_7$ secondary crystalline phases were detected in post heat-treated SYb and SY specimens, respectively, in addition to β-Si_3N_4. It has been reported that the melting point of $Yb_2Si_2O_7$ and $Y_2Si_2O_7$ are 1850°C [32] and 1775°C [33], respectively. It indicated that $Yb_2Si_2O_7$ is more refractory than $Y_2Si_2O_7$.

The grain boundary phases of post heat-treated SY and SYB samples were examined by HRTEM with results shown in Fig. 8. Amorphous films with thickness of 1.3 and 1.0 nm were observed in SY and SYb samples, respectively. The thickness of the intergranular film was determined by a balance of attractive and repulsive forces [12,34]. The attractive term that acts to draw the grains together is composed of van der Waals dispersion force and a capillary pressure. The repulsive term could be the steric force and the contribution of the electrical double layer. Wang [35] reported that the increase in

ionic radius of the rare-earth additives, the decrease in the attractive force and, concurrently, the increase in the repulsive force could result in the films observed in Fig. 8. The thicker amorphous films in SY samples were therefore probably due to the relatively larger radius of Y (0.90 Å) than that of Yb (0.87 Å). Both the film thickness and characteristics of glass phase could be related to the high-temperature mechanical properties of Si_3N_4 [35].

The SEM micrographs of as-sintered SYb specimens fractured respectively at 1200 and 1400°C are shown in Fig. 9a and b. Typical brittle cleavage fracture mode with voids due to pullout of elongated grains was observed on fractured surface of as-sintered specimens tested at 1200°C (Fig. 9a). At 1400°C, however, the pullout voids had a tendency of being filled out by the amorphous melt and, therefore, the fractured surface appeared flat (Fig. 9b). This observation suggested that the softening of intergranular phases at elevated temperatures could be responsible for the degradation of strength [36].

The fractured surface of post heat-treated SYb specimens, tested at 1400°C is further shown in Fig. 9c. Different from what was observed in the as-sintered specimens (Fig. 9b), voids due to pullout of elongated grains and intergranular fracture mode can be observed. In addition, a relatively rough surface and voids adhering with a

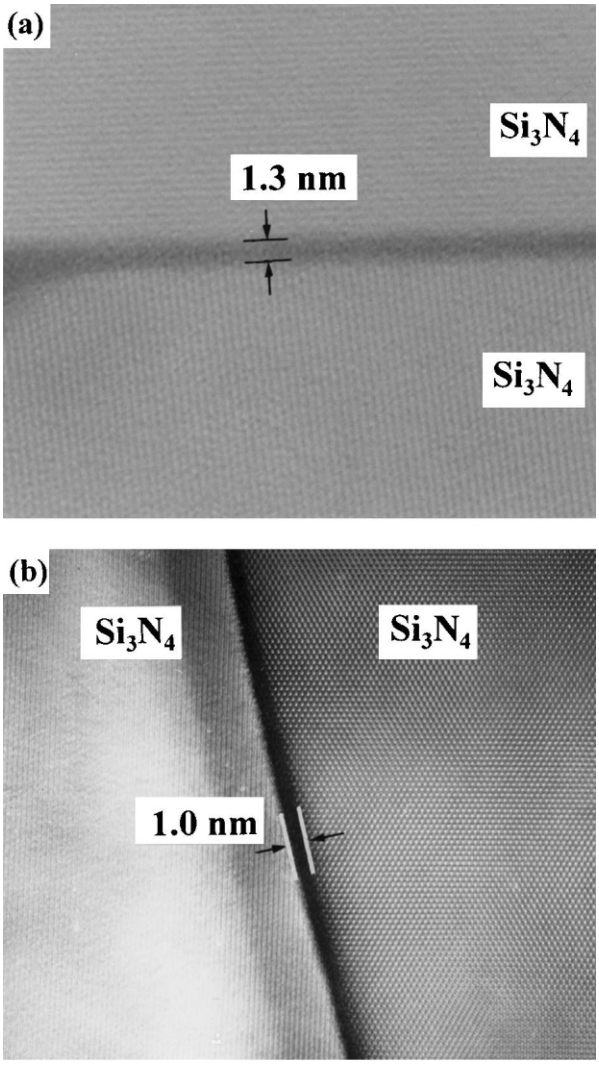

Fig. 8. HRTEM lattice images of post heat-treated specimens showing the intergranular amorphous films of (a) SY, (b) SYb.

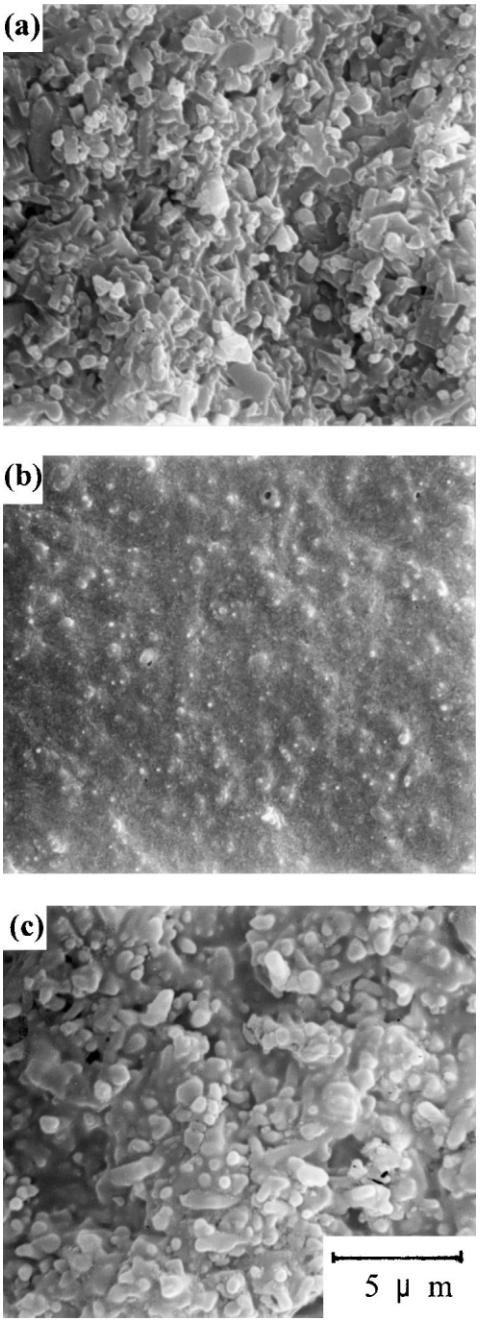

Fig. 9. SEM micrographs showing the fractured surfaces of SYb specimens: (a) as-sintered SYb samples after being tested at 1200°C; (b) as-sintered SYb samples after being tested at 1400°C; (c) post heat-treated SYb samples after being tested at 1400°C.

trace of solidified melt are noticed. These observations suggested that the crystallization of grain boundary phases after heat treatment could change the interfacial bonding and enhance the high temperature strength

4. Conclusions

1. The sinterability and α to β phase transformation of the specimens with Y_2O_3 were higher than those with Yb_2O_3 with the same content of additives.
2. Wider grain width distribution and larger grain width were observed in the specimens with Y_2O_3 than those with Yb_2O_3.
3. The specimens with Yb_2O_3 have higher flexure strength, hardness and fracture toughness.
4. The crystallization of the intergranular phase, and control of the refractoriness and film thickness of residual grain boundary phases could achieve high strength retention at elevated temperatures.

Acknowledgements

The authors would like to thank the National Science Council of the Republic of China for its financial support under contract No. NSC 89-2216-E006-034.

References

[1] C.J. Hwang, T.Y. Tien, Microstructural development in silicon nitride ceramics, Mater. Sci. Forum 47 (1989) 84–109.
[2] P.F. Becher, H.T. Lin, S.L. Hwang, M.J. Hoffmann, I.W. Chen, The influence of microstructure on the mechanical behavior of silicon nitride ceramics, in: I.W. Chen, P.F. Becher, M. Mitomo, G. Petzow, T.S. Yen (Eds.), Silicon Nitride Ceramics — Scientific and Technological Advances, Proceeding of the Materials Research Society Symposium, Vol. 287, Boston, MA, December 1992, Materials Research Society, Pittsburgh, PA, 1993, pp. 147–158.
[3] T. Nishimura, M. Mitomo, H. Suematsu, High temperature strength of silicon nitride ceramics with ytterbium silicon oxynitride, J. Mater. Res. 12 (1) (1997) 203–209.
[4] C.M. Wang, X.Q. Pan, M. Rühle, F.L. Riley, M. Mitomo, Review: silicon nitride crystal structure and observations of lattice defects, J. Mater. Sci. 31 (1996) 5281–5298.
[5] R.A. German, Liquid Phase Sintering, Plenum Press, New York, 1985, pp. 127–155.
[6] N. Hirosaki, A. Okada, K. Matoba, Sintering of Si_3N_4 with the addition of rare-earth oxides, J. Am. Ceram. Soc. 71 (3) (1988) c-144–c-147.
[7] N. Hirosaki, Y. Okamoto, Y. Akimune, M. Mitomo. Sintering of Y_2O_3–Al_2O_3-doped β-Si_3N_4 powder and mechanical properties of sintered materials, J. Ceram. Soc. Jpn., Int. Ed. 102 (1994) 791–795.
[8] D.R. Clarke, G. Thomas, Microstructure of Y_2O_3 fluxed hot-pressed silicon nitride, J. Am. Ceram. Soc. 61 (3–4) (1978) 114–118.
[9] Y. Goto, G. Thomas, Microstructure of silicon nitride ceramics sintered with rare-earth oxide, Acta Metall. Mater. 43 (3) (1995) 923–930.
[10] K.S. Mazdiyasni, C.M. Cooke, Consolidation, microstructure, and mechanical properties of Si_3N_4 doped with rare-earth oxides, J. Am. Ceram. Soc. 57 (12) (1974) 536–537.
[11] O.L. Krivanek, T.M. Shaw, G. Thomas, The microstructure and distribution of impurities in hot-pressed and sintered silicon nitride, J. Am. Ceram. Soc. 62 (11–12) (1979) 585–590.
[12] D.R. Clarke, On the equilibrium thickness of intergranular glass phases in ceramic materials, J. Am. Ceram. Soc. 70 (1) (1987) 15–22.
[13] A. Tsuge, K. Nishida, M. Komatsu, Effect of crystallizing the grain-boundary glass phase on the high-temperature strength of hot-pressed Si_3N_4 containing Y_2O_3, J. Am. Ceram. Soc. 58 (7–8) (1975) 323–326.
[14] M.K. Cinibulk, G. Thomas, S.M. Johnson, Fabrication and secondary-phase crystallization of rare-earth disilicate-silicon nitride ceramics, J. Am. Ceram. Soc. 75 (8) (1992) 2037–2043.
[15] M.K. Cinibulk, G. Thomas, S.M. Johnson, Strength and creep behavior of rare-earth disilicate silicon nitride ceramics, J. Am. Ceram. Soc. 75 (8) (1992) 2050–2055.
[16] D.M. Mieskowski, W.A. Sanders, Oxidation of silicon nitride sintered with rare-earth oxide additions, J. Am. Ceram. Soc. 68 (7) (1985) c-160–c-163.
[17] G. Woetting, B. Kanka, G. Ziegler, Microstructural development, microstructural characterization and relation to mechanical properties of dense silicon nitride, in: S. Hampshire (Ed.), Non-Oxide Technical and Engineering Ceramics, Elsevier Applied Science, London and New York, 1986, pp. 83–96.
[18] C.P. Gazzara, D.R. Messier, Determination of phase content of Si_3N_4 by X-ray diffraction analysis, Ceram. Bull. 56 (9) (1977) 777–780.
[19] T. Nose, T. Fujii, Evaluation of fracture toughness for ceramic materials by a single-edge-precracked-beam method, J. Am. Ceram. Soc. 71 (5) (1988) 328–333.
[20] Y. Goto, G. Thomas, Phase transformation and microstructural changes of Si_3N_4 during sintering, J. Mater. Sci. 30 (1995) 2194–2200.
[21] H.-H. Lu, J.-L. Huang, Microstructure in silicon nitride containing β-phase seeding, Part 1, J. Mater. Res. 14 (7) (1999) 2966–2973.
[22] V.K. Sarin, On the α-to-β phase transformation in silicon nitride, Mater. Sci. Eng. A105/106 (1988) 151–159.
[23] D.D. Lee, S.J.L. Kang, G. Petzow, D.N. Yoon, Effect of α to β(β′) phase transition on the sintering of silicon nitride ceramics, J. Am. Ceram. Soc. 73 (3) (1990) 767–769.
[24] J.E. Shelby, J.T. Kohli, Rare-earth aluminosilicate glasses, J. Am. Ceram. Soc. 73 (1) (1990) 39–42.
[25] Y. Tajima, Development of high performance silicon nitride ceramics and their application, Mater. Res. Symp. Proc. 287 (1993) 189–197.
[26] E. Meibner, H.J. Kleebe, G. Ziegler, Influence of post-sintering anneal on Si_3N_4 matrix-grain morphology, in: P. Duran, J.F. Fernandez (Eds.), Third Euro-ceramics, 1993, vol. 3, pp. 397–403.
[27] M.J. Hoffmann, G. Petzow, Microstructural design of Si_3N_4-based ceramics, in: I.W. Chen, P.F. Becher, M. Mitomo, G. Yen, T.S. Yen (Eds.), Silicon Nitride Ceramics — Scientific and Technological Advances, Proceeding of the Materials Research Society Symposium, Vol. 287, Boston, MA, December 1992, Materials Research Society, Pittsburgh, PA, 1993, pp. 3–15.
[28] K. Hirao, T. Nagaoka, M.E. Brito, S. Kanzaki, Mechanical properties of silicon nitrides with tailored microstructure by seeding, J. Ceram. Soc. Jpn 104 (1) (1996) 54–58.
[29] H. Park, H.E. Kim, K. Niihara, Microstructural evolution and mechanical properties of Si_3N_4 with Yb_2O_3 as a sintering additive, J. Am. Ceram. Soc. 80 (3) (1997) 750–756.
[30] M.K. Cinibulk, G. Thomas, S.M. Johnson, Grain-boundary-phase crystallization and strength of silicon nitride sintered with a YSiAlON glass, J. Am. Ceram. Soc. 73 (6) (1990) 1606–1612.

[31] B. Budiansky, J.W. Hutchinson, A.G. Evans, Matrix fracture in fiber-reinforced ceramics, J. Mech. Phys. Solids 34 (2) (1986) 167–189.
[32] E.M. Levin, C.R. Robbins, H.F. McMurdie, Phase diagram for ceramists 1969 supplement, The American Ceramic Society, Westerville, OH, 1969, p. 108.
[33] E.M. Levin, C.R. Robbins, H.F. McMurdie, Phase diagram for ceramists 1969 supplement, The American Ceramic Society, Westerville, OH, 1969, p. 107.
[34] D.R. Clarke, T.M. Shaw, A.P. Philipse, R.G. Horn, Possible electrical double layer contribution to the equilibrium thickness of intergranular glass films in polycrystalline ceramics, J. Am. Ceram. Soc. 76 (1993) 1201–1204.
[35] C.M. Wang, X. Pan, M.J. Hoffmann, R.M. Cannon, M. Rühle, Grain boundary films in rare-earth-glass based silicon nitride, J. Am. Ceram. Soc. 79 (3) (1996) 788–792.
[36] J.L. Huang, Z.H. Shih, H.H. Lu, C.Y. Chen, The effects of post heat-treatment on the microstructure and fracture behaviors of Yb_2O_3-doped Si_3N_4, Mater. Chem. Phys. 63 (2000) 116–121.